Developmental Cell
Article

The Conserved Protein SZY-20 Opposes the Plk4-Related Kinase ZYG-1 to Limit Centrosome Size

Mi Hye Song,[1,*] L. Aravind,[2] Thomas Müller-Reichert,[3] and Kevin F. O'Connell[1,*]
[1]Laboratory of Biochemistry and Genetics, National Institute of Diabetes and Digestive and Kidney Diseases
[2]National Center for Biotechnology Information, National Library of Medicine
National Institutes of Health, Bethesda, MD 20894, USA
[3]Max Planck Institute of Molecular, Cell Biology and Genetics (MPI-CBG), Pfotenhauerstrasse 108, 01307 Dresden, Germany
*Correspondence: mihyesong@mail.nih.gov (M.H.S.), kevino@intra.niddk.nih.gov (K.F.O.)
DOI 10.1016/j.devcel.2008.09.018

SUMMARY

Microtubules are organized by the centrosome, a dynamic organelle that exhibits changes in both size and number during the cell cycle. Here we show that SZY-20, a putative RNA-binding protein, plays a critical role in limiting centrosome size in *C. elegans*. SZY-20 localizes in part to centrosomes and in its absence centrosomes possess increased levels of centriolar and pericentriolar components including γ-tubulin and the centriole duplication factors ZYG-1 and SPD-2. These enlarged centrosomes possess normal centrioles, nucleate more microtubules, and fail to properly direct a number of microtubule-dependent processes. Depletion of ZYG-1 restores normal centrosome size and function to *szy-20* mutants, whereas loss of *szy-20* suppresses the centrosome duplication defects in both *zyg-1* and *spd-2* mutants. Our results describe a pathway that determines centrosome size and implicate centriole duplication factors in this process.

INTRODUCTION

The centrosome serves as the primary microtubule-organizing center (MTOC) in animal cells. In this capacity, the centrosome participates in many processes, including assembly and positioning of the mitotic spindle, chromosome segregation, and cytokinesis. The centrosome consists of a pair of centrioles surrounded by a mass of pericentriolar material (PCM) (Luders and Stearns, 2007). Centrioles are barrel-shaped structures, composed of a 9-fold radial symmetric array of microtubules and are structurally similar to the basal bodies that organize the microtubules of cilia and flagella. By contrast, the structure of the PCM is not well defined, but is enriched in coiled-coil proteins that are thought to form a framework that supports microtubule nucleation and anchoring (Azimzadeh and Bornens, 2007).

To ensure spindle bipolarity and the proper transmission of centrioles, the centrosome must be duplicated precisely once per cell cycle. The central event in centrosome duplication is the assembly of a single daughter centriole next to each preexisting (mother) centriole. Recent work indicates that the molecular pathway of centriole assembly is similar in humans and worms, and relies upon a conserved set of core duplication factors (Delattre et al., 2006; Kleylein-Sohn et al., 2007; Pelletier et al., 2006). In *C. elegans*, the kinase ZYG-1 (O'Connell et al., 2001), a relative of human Plk4 and *Drosophila* Sak (Bettencourt-Dias et al., 2005; Habedanck et al., 2005) localizes early to the site of centriole assembly (Delattre et al., 2006; Pelletier et al., 2006) and is required to recruit a series of coiled-coil proteins including SAS-4 (Kirkham et al., 2003; Leidel and Gonczy, 2003), SAS-5 (Delattre et al., 2004), and SAS-6 (Dammermann et al., 2004; Leidel et al., 2005). Likewise, during centriole assembly in human cells, Plk4 recruits orthologs of SAS-4 and SAS-6 (Kleylein-Sohn et al., 2007).

Centrosome duplication in *C. elegans* also requires the activity of another conserved factor called SPD-2 (Kemp et al., 2004; Pelletier et al., 2004). SPD-2 is a component of both PCM and centrioles, and has a conserved role in PCM assembly (Dix and Raff, 2007; Giansanti et al., 2008; Gomez-Ferreria et al., 2007; Kemp et al., 2004; Pelletier et al., 2004; Zhu et al., 2008). During centrosome duplication in *C. elegans*, SPD-2 is required to localize ZYG-1 to sites of centriole assembly (Delattre et al., 2006; Pelletier et al., 2006). Yet SPD-2 does not appear to be required for centrosome duplication in flies (Dix and Raff, 2007; Giansanti et al., 2008), and in humans this role remains controversial (Gomez-Ferreria et al., 2007; Zhu et al., 2008). Thus, the role of SPD-2 in centrosome duplication does not appear to be absolutely conserved, suggesting that in some species ZYG-1 homologs can localize independently of SPD-2.

Recent studies indicate that the PCM plays a role in daughter centriole assembly. In worms, depletion of PCM components such as γ-tubulin and the coiled-coil protein SPD-5 inhibits daughter centriole formation (Dammermann et al., 2004), while in vertebrates experimental expansion of the PCM promotes the formation of multiple daughter centrioles (Loncarek et al., 2008). These results indicate that the PCM provides an environment favorable for centriole assembly. Conversely, centrioles organize PCM. Disruption of centrioles in human cells results in dispersion of the PCM, suggesting that the centriole possesses a PCM-organizing activity (Bobinnec et al., 1998). This is supported by work in *C. elegans* where partial depletion of centriole duplication factors has been shown to lead to partial assembly of centrioles and a corresponding reduction in PCM, suggesting that a centriole-associated activity determines centrosome size

(Delattre et al., 2004; Kirkham et al., 2003; Leidel et al., 2005). What this activity is and how centrosome size is determined remain unclear.

Here we have identified a conserved protein, SZY-20, that limits the size of centrosomes in *C. elegans* embryos. Loss of SZY-20 activity results in an approximately 2-fold increase in the amounts of centrosome-associated ZYG-1, SPD-2, SPD-5, and γ-tubulin. This increase in centrosome size is associated with an increase in microtubule-nucleating capacity, defects in microtubule-dependent processes, and embryonic lethality. Reducing ZYG-1 activity in *szy-20* mutants restores centrosome size, normal microtubule function, and to some extent embryonic viability, indicating that the level of centriole-associated ZYG-1 determines centrosome size. We also find that centrosome size is influenced by SAS-6 activity.

RESULTS

SZY-20 Is a Negative Regulator of Centrosome Duplication

The *szy-20* gene was identified in a screen for genetic suppressors of the temperature-sensitive (ts) lethality of the *zyg-1(it25)* mutation (Kemp et al., 2007). In *zyg-1(it25)* embryos raised at the restrictive temperature (24°C), duplication of the sperm-derived centriole pair invariably fails. This initial centriole pair, however, is able to separate and direct formation of a bipolar spindle. Such embryos divide once to form a two-cell embryo, but during the second round of mitosis, each blastomere assembles a monopolar spindle (Figure 1A). As a result, 100% of the embryos die (O'Connell et al., 2001). The *szy-20(bs52)* mutation, however, suppresses the embryonic lethality of *zyg-1(it25)* such that a percentage of double-mutant embryos are able to complete development and hatch at the restrictive temperature (Table 1, top). Importantly, the *szy-20(bs52)* mutation is unable to suppress a complete loss of *zyg-1* activity, indicating that suppression might involve upregulation of ZYG-1 (Kemp et al., 2007).

To investigate the basis of suppression, we analyzed bipolar spindle formation and centrosome duplication directly in *zyg-1(it25) szy-20(bs52)* double-mutant embryos. By four-dimensional differential interference contrast (4D-DIC) imaging (Figure 1A; see Movie S1 available online), we found that *zyg-1(it25) szy-20(bs52)* embryos are often successful in assembling bipolar spindles at the two-cell stage (13/24 events), unlike *zyg-1(it25)* embryos (0/28 events). The ability of the double mutant to assemble bipolar spindles appears to result from suppression of the centrosome duplication defect, as spindle poles in *zyg-1(it25) szy-20(bs52)* embryos invariably stained with the centriole marker SAS-4 (Figure 1B). The ability of the *szy-20(bs52)* mutation to suppress the centrosome duplication defect was further confirmed by fluorescence imaging of live embryos expressing GFP-SPD-2 to mark centrosomes and GFP-histone to mark DNA (Figure 1C and Movie S2). As *szy-20(bs52)* is a loss-of-function allele (see below), our results demonstrate that *szy-20* negatively regulates centriole assembly.

The *szy-20(bs52)* Mutation Restores Centrosome Duplication in *spd-2* Mutants

We next asked if the *szy-20(bs52)* mutation could also suppress mutations in other genes required for centrosome duplication.

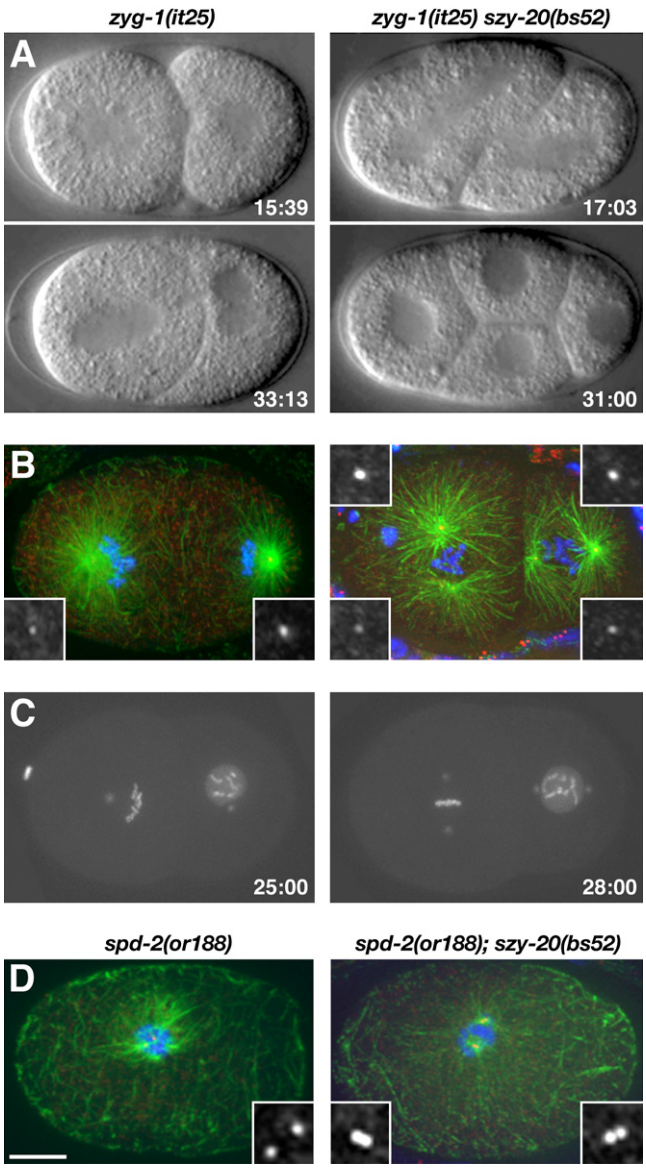

Figure 1. Loss of *szy-20* Activity Suppresses Centrosome Duplication Defects in *zyg-1* and *spd-2* Mutants

(A–C) Centrosome duplication and bipolar spindle formation are restored in *zyg-1(it25) szy-20(bs52)* embryos. (A) Selected images from 4D-DIC recordings. Only the double-mutant embryo progresses to the four-cell stage. (B) Two-cell stage embryos stained for microtubules (green), centrioles (SAS-4, red), and DNA (blue). (C) Selected images from recordings of embryos expressing GFP-SPD-2 and GFP-histone. Time (minutes) is relative to first metaphase.

(D) One-cell embryos stained for microtubules (green), SAS-4 (red), and DNA (blue). The *spd-2(or188)* embryo has two centrioles and the *spd-2(or188) szy-20(bs52)* embryo four. Each image is a Z projection. Insets are magnified 3-fold. Bar, 10 μm.

spd-2 is required for both centrosome duplication and PCM assembly. In *spd-2* mutants, the sperm-derived centriole pair fails to duplicate and only weakly organizes microtubules (Kemp et al., 2004; Pelletier et al., 2004). As a result, *spd-2* mutants fail to assemble the first mitotic spindle, and they arrest at the one-cell stage. We generated a double-mutant line and found

Table 1. Genetic Analysis of *szy-20*

	°C	% Embryonic Viability (Average ± SD)	N[a]
Depletion of *szy-20* Suppresses *zyg-1* Mutations			
zyg-1(it25)	24	0 ± 0	352
zyg-1(it25) szy-20(bs52)	24	4.7 ± 2.1	618
zyg-1(it25) RNAi neg control[b]	24	0 ± 0	200
zyg-1(it25) C18E9.3 RNAi	24	2.6 ± 2.6	2467
zyg-1(or409) RNAi neg control[b]	24	0 ± 0	466
zyg-1(or409) C18E9.3 RNAi	24	8.2 ± 9.7	1952
zyg-1(it25) RNAi neg control[b]	23.5	0.3 ± 0.003	752
zyg-1(it25) C18E9.3 RNAi	23.5	27.2 ± 18.7	1123
zyg-1(it25)	20	96.2 ± 2.5	909
szy-20(bs52)	20	55.0 ± 8.7[c]	909
zyg-1(it25) szy-20(bs52)	20	92.1 ± 3.3[c]	900
szy-20 Is Required for Embryogenesis			
szy-20(bs52)	20	55.0 ± 8.7	909
szy-20(tm1997)	20	63.2 ± 10.0	199
C18E9.3 RNAi	20	92.3 + 8.4	1315
szy-20(bs52) C18E9.3 RNAi	20	4.8 ± 6.6	380
szy-20(bs52)	24	24.6 ± 13.0	668
szy-20(tm1997)	24	23.1 ± 17.9	324
szy-20(bs52)	25	1.3 ± 0.7	152
szy-20(bs52)/+	25	99.6 ± 0.9	224
szy-20(tm1997)	25	0.4 ± 0.9	261
szy-20(bs52)/szy-20(tm1997)	25	3.9 ± 4.8	573
+/mnDf68[d]	25	55.4 ± 24.2	428
szy-20(bs52)/mnDf68[d]	25	4.5 ± 8.3	620
+/mnDf104[e]	25	66.7 ± 7.6	696
szy-20(bs52)/mnDf104[e]	25	61.1 ± 9.5	1657
N2	25	99.9 ± 0.1	202
RNAi neg control[b]	25	99.7 ± 0.5	505
C18E9.3 RNAi	25	13.6 ± 8.1	902

[a] Number of embryos scored.
[b] For negative controls for RNAi soaking experiments, animals were incubated in M9 buffer lacking RNA.
[c] p value = 0.0069 (Student's t test; two-tailed distribution and two-sample equal variance).
[d] The deficiency chromosome *mnDf68* carries a large deletion of LG II that encompasses ORF C18E9.3.
[e] The deficiency chromosome *mnDf104* carries a large deletion of LG II that does not encompass ORF C18E9.3.

that the *szy-20(bs52)* mutation only weakly suppresses the embryonic lethality of the hypomorphic *spd-2(or188)* mutation (data not shown). When we examined the *spd-2(or188); szy-20(bs52)* double mutant by immunofluorescence microscopy, we found that the microtubule organization and one-cell arrest phenotypes were still present. However, as judged by SAS-4 immunostaining, the double-mutant embryos exhibited evidence of centrosome duplication (Figure 1D). While only 7% of one-cell *spd-2(or188)* embryos (n = 28) possessed more than the two original sperm-derived centrioles, 65% of *spd-2(or188); szy-20(bs52)* embryos (n = 45) possessed three or more centrioles. Thus, *szy-20* genetically interacts with *zyg-1* and *spd-2*, two genes whose products function at the earliest known step in centrosome duplication (Delattre et al., 2006; Pelletier et al., 2006).

As a control we assayed the ability of the *szy-20(bs52)* mutation to suppress an unrelated ts mutant. At 24°C, the *mat-3(or180)* mutation blocks the function of the anaphase-promoting complex, producing an embryonic lethal phenotype marked by a one-cell arrest (Stein et al., 2007). Analysis of a *szy-20(bs52); mat-3(or180)* double mutant revealed that *szy-20(bs52)* suppresses neither the embryonic lethal phenotype nor the one-cell arrest of *mat-3(or180)* mutants (data not shown), indicating that *szy-20(bs52)* is not a general suppressor of ts mutations.

Maternally Supplied SZY-20 Is Essential for Embryonic Development

The *szy-20(bs52)* mutation confers its own recessive ts embryonic lethal phenotype (Table 1, bottom; Kemp et al., 2007). At 20°C, greater than 50% of the progeny of *szy-20(bs52)* hermaphrodites are viable, but at 25°C nearly all of the progeny fail to hatch. As the embryonic lethality of *szy-20(bs52)* hermaphrodites cannot be rescued by mating to wild-type males (data not shown), maternally expressed SZY-20 is essential for embryogenesis.

Preliminary analysis of *szy-20(bs52)* embryos revealed defects in cytokinesis and in attachment of the centrosome to the nucleus (Kemp et al., 2007). To further characterize the consequences of loss of *szy-20*, we analyzed a large number of *szy-20(bs52)* embryos stained for microtubules, DNA, and centrosomes (Figure 2). At 25°C, *szy-20(bs52)* embryos exhibit multiple defects in cell division. As observed previously, some embryos contain extra nuclei and centrosomes, a phenotype suggestive of cytokinesis failure (20%, n = 135; Figure 2A), while in others centrosomes lose contact with the nuclear envelope (12%, n = 135; Figure 2B). We also observed defects that had not been previously observed. *szy-20(bs52)* embryos exhibit a 10% decrease in the length of metaphase spindles compared to wild-type embryos (n = 12; Figure 4D). We also noticed the presence of more than one sperm pronucleus-centrosome pair in a small fraction (<5%) of embryos, a phenotype suggestive of polyspermy (Figure 2C).

To further define *szy-20* function, we performed live imaging of *szy-20(bs52)* embryos grown at 25°C (Movies S3 and S4). Time-lapse recordings confirmed a cytokinesis defect in *szy-20(bs52)* embryos. In these embryos, the furrow initiates normally but fails to ingress completely, resulting in the formation of a multinucleated cell with four centrosomes. *szy-20(bs52)* embryos also frequently fail to extrude polar bodies and exhibit a slight (1.2- to 1.4-fold) lengthening of the cell cycle. While these defects are observed at all temperatures, the severity and penetrance of each defect increases at higher temperature. We also analyzed the deletion allele *szy-20(tm1997)* and found that it confers a ts embryonic lethal phenotype and many of the cytological defects described for *szy-20(bs52)* (Table 1, bottom, and data not shown).

Molecular Characterization of *szy-20*

To further define the role of SZY-20, we sought to clone the corresponding gene located between *dpy-10* and *unc-4* on chromosome II (Kemp et al., 2007). Using a physical mapping approach,

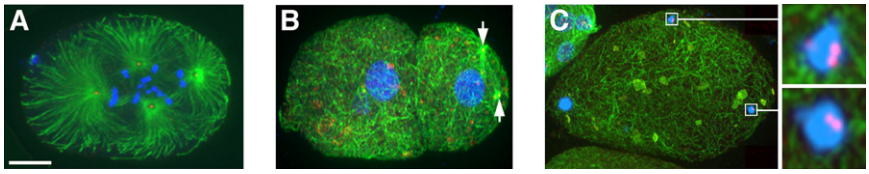

Figure 2. SZY-20 Is Required for Cell Division

szy-20(bs52) embryos stained for microtubules (green), centrosomes (red), and DNA (blue).

(A) A one-cell embryo with four centrosomes stained for ZYG-1.

(B) A two-cell embryo with detached centrosomes (arrows) stained for SPD-2.

(C) A zygote with two sperm pronuclei and centrosomes (boxed) stained for SAS-4. Each image is Z projection. Insets are magnified 3-fold. Bar, 10 μm.

we localized *szy-20* to a small interval of 54.2 kb that encompasses 14 predicted open reading frames (ORFs; Figure S1). Sequencing detected a nonsense (C-to-T) mutation in exon 6 of ORF C18E9.3 that presumably results in truncation of the gene product (Figure 3A and Figure S1).

To confirm the identity of *szy-20*, we used RNAi to inhibit expression of C18E9.3 in both wild-type and *zyg-1(it25)* animals. In all respects, C18E9.3 RNAi phenocopied the *szy-20(bs52)* mutation. C18E9.3 RNAi partially suppressed *zyg-1(it25)* embryonic lethality (Table 1, top); this was most obvious at 23.5°C, where C18E9.3 RNAi of *zyg-1(it25)* animals led to a 100-fold increase in the frequency of viable progeny (27.2% versus 0.27% in controls). C18E9.3 RNAi also suppressed the embryonic lethality of the *zyg-1(or409)* allele. In wild-type animals, C18E9.3 RNAi produced a ts embryonic lethal phenotype reminiscent of *szy-20(bs52)*: <10% embryonic lethality at 20°C, but ~90% at 25°C (Table 1, bottom). Further, combining the mutation and RNAi had a synergistic effect at 20°C: only ~5% of the progeny of *szy-20(bs52)* C18E9.3 RNAi mothers survived, compared to 55% for *szy-20(bs52)* and 92.3% for C18E9.3 RNAi. Finally, *szy-20(bs52)* failed to complement *szy-20(tm1997)*, a partial deletion of C18E9.3 (Table 1, bottom). We conclude that *szy-20* corresponds to ORF C18E9.3. Based on the ability to phenocopy *szy-20(bs52)* by RNAi as well as the failure of *szy-20(bs52)* to complement *mnDf68*, a chromosomal deficiency that removes the *szy-20* locus (Table 1, bottom), we conclude that *szy-20(bs52)* is a loss-of-function allele.

Wormbase (http://www.wormbase.org/) lists multiple ESTs for C18E9.3. We sequenced four of these cDNA clones and identified two alternatively spliced transcripts (Figure S1). The longer transcript encodes a protein of 558 amino acids (Isoform A; GenBank accession EF656060) and the shorter transcript a protein of 457 amino acids (Isoform B; GenBank accession EF656061). Both messages are *trans*-spliced to the SL1 leader sequence and appear to utilize the same initiation and termination codons.

szy-20 Encodes a Conserved Protein

A BLAST search (Experimental Procedures) identified SZY-20 orthologs in other species including flies and humans. All animal genomes with significant sequence data contain one ortholog of

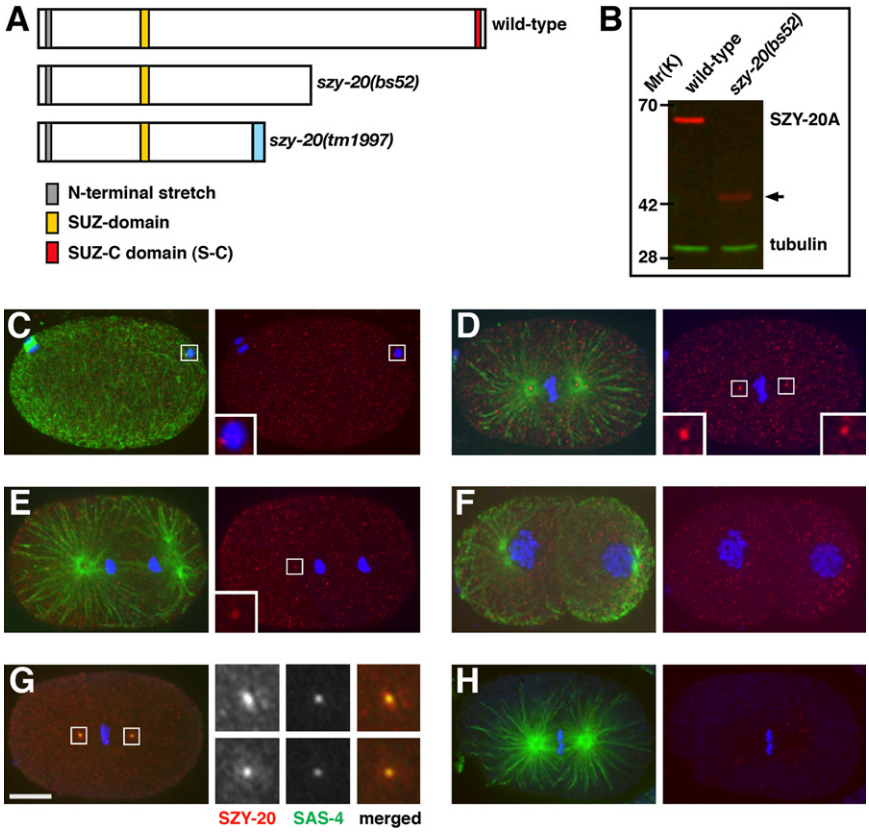

Figure 3. *szy-20* Encodes a Conserved Protein

(A) Schematic of wild-type and mutant forms of SZY-20. Due to a frame shift, the product of the *szy-20(tm1997)* allele is expected to contain a novel 36 amino acid extension (blue box).

(B) Immunoblot of wild-type and *szy-20(bs52)* embryonic extracts probed for SZY-20 (red), and α-tubulin (green) as a loading control.

(C–H) SZY-20 localizes to the centrosome. Embryos stained for microtubules (green), SZY-20 (αS20N, red), and DNA (blue). Wild-type embryos at (C) meiosis, (D) first metaphase, (E) first anaphase, (F) second interphase, and (H) a *szy-20(RNAi)* embryo at metaphase. (G) A metaphase embryo costained for SZY-20 (red) and GFP-SAS-4 (green). Boxes highlight centrosomes. Insets are magnified 3-fold. Bar, 10 μm.

SZY-20, indicating a potentially conserved role across animals. A multiple alignment of SZY-20 with its homologs showed that they all share three prominent blocks of conservation (Figure 3A and Figure S2). The N-terminal block is a short element with a characteristic hx[DE][SN]W[DE][DE] signature (where h is any hydrophobic residue and x is any residue), which is found exclusively in orthologs of SZY-20 (Figure S2A). The second block in the center of the protein, termed the SUZ domain, is the strongest stretch of conservation and is enriched in charged residues (Figure S2B). The third block, the SUZ-C domain, is at the extreme C terminus and is defined by a characteristic pattern of two highly conserved glycines and one absolutely conserved proline (Figure S2C). In nematodes, however, this domain has rapidly diverged.

We noticed that the SUZ and SUZ-C domains occur independently in proteins outside of the SZY-20 family (Figure S3 and Supplemental Results). Interestingly, many of these proteins contain known RNA-binding domains, suggesting that SZY-20 might function in RNA metabolism. We tested SZY-20 for RNA binding in vitro. GST-SZY-20 specifically and reproducibly coprecipitates with polyuridine-coupled beads, indicating that SZY-20 can directly bind RNA (Figure S4A). Both the SUZ and SUZ-C domains contribute to this activity, as mutation of either domain significantly reduces the ability of the protein to coprecipitate with the beads. Furthermore, RNA binding is nearly eliminated in a double mutant (GST-SZY-20^{dm}) that carries mutations in both domains (Figure S4B). To investigate the function of these putative RNA-binding domains in vivo, we expressed FLAG-tagged versions of wild-type and SZY-20^{dm} in worms (Figure S4C). When expressed in *szy-20(bs52)* animals grown at 25°C, the wild-type FLAG-SZY-20 protein provided strong rescue of the embryonic lethality, reducing it to 52% (n = 2615) from 96% in controls (n = 936). In contrast, the FLAG-SZY-20^{dm} mutant had little effect (84% embryonic lethality, n = 1215), consistent with the notion that RNA binding is involved in SZY-20 function.

SZY-20 Localizes to Nuclei, Cytoplasm, and Centrosomes

To determine how SZY-20 might function, we examined its subcellular distribution by using affinity-purified antibodies. On immunoblots, the αS20N antibody detected a single band in wild-type embryonic extracts. The migration of this band was consistent with the size of isoform A (Figure 3B). This band was absent in *szy-20(bs52)* embryonic extracts. Instead a faster migrating band, presumably corresponding to the truncated product, was detected.

In immunostained embryos, SZY-20 is found in small foci in the cytoplasm and at centrosomes where it coincides with GFP-SAS-4, a marker of centrioles (Figures 3C–3G). In addition, SZY-20 localizes to nucleoli during interphase and to the surface of chromosomes during meiosis and mitosis (Figure S5). RNAi of *szy-20* significantly reduces staining of all structures, confirming the specificity of the antibody (Figure 3H). SZY-20 is first detected at centrosomes during meiosis, where it often appears as two distinct dots adjacent to the male pronucleus (Figure 3C). While SZY-20 localizes to the centrosome throughout the cell cycle, the extent of its association is regulated in a cell-cycle-dependent manner (Figures 3C–3F). The level of centrosome-associated SZY-20 peaks at prometaphase and metaphase, slowly declines, and reaches a minimal level during interphase. In contrast, the level of ZYG-1 at centrosomes is lowest at metaphase (Delattre et al., 2006), the time when the level of SZY-20 peaks. ZYG-1 then rapidly increases during anaphase while SZY-20 levels drop. This reciprocal relationship between centrosomal levels of SZY-20 and ZYG-1 suggests that SZY-20 acts locally to regulate ZYG-1.

SZY-20 Limits Centrosome Size

During our cytological characterization, we noticed that centrosomes appear larger in *szy-20(bs52)* than in wild-type embryos. This difference was apparent in embryos stained for the pericentriolar component SPD-5 (Figure 4A). We measured the fluorescence intensity of stained centrosomes at first metaphase (Figure 4B) and found that *szy-20(bs52)* embryos (n = 31) contain more than twice as much centrosomal SPD-5 as controls (n = 10). In contrast, cytoplasmic pools of SPD-5 appear similar in the two strains, suggesting that the overall levels of SPD-5 are unaffected by the *szy-20(bs52)* mutation. This was confirmed by quantitative immunoblotting (Figure 4C), which showed that wild-type and mutant embryos possessed similar amounts of SPD-5 (mutant/wt = 1.12 ± 0.09, n = 4). This result suggests that the *szy-20(bs52)* mutation might enhance recruitment of SPD-5 to centrosomes.

SPD-2 and SPD-5 function at the top of a hierarchy in the centrosome maturation pathway (Hamill et al., 2002; Kemp et al., 2004; Pelletier et al., 2004). In addition to recruiting downstream components, SPD-2 and SPD-5 localize to PCM in a mutually dependent manner. We postulated that the *szy-20(bs52)* mutation would affect the level of SPD-2 at centrosomes and analyzed embryos expressing GFP-SPD-2 (Figure 4D). As predicted, the level of centrosome-associated GFP-SPD-2 is significantly increased in the *szy-20(bs52)* mutant at all stages of the cell cycle. The increase in centrosomal levels of GFP-SPD-2 reflects increases in both density (1.4 ± 0.6 fold) and cross-sectional area (1.4 ± 0.5 fold). However, we detected no significant difference in overall levels of endogenous SPD-2 between wild-type and *szy-20(bs52)* embryos (mutant/wt = 1.08 ± 0.14, n = 5), as shown in Figure 4E. Thus, the elevated levels of SPD-5 and SPD-2 at mutant centrosomes most likely result from enhanced recruitment.

To further confirm the role of SZY-20 in regulating centrosome size, we overexpressed SZY-20 in wild-type embryos (Figure 4F). Consistent with a role as a negative regulator, overexpression of wild-type FLAG-SZY-20 reduces the centrosomal level of GFP-SPD-2 by half (0.48 ± 0.1 fold, n = 11) compared to controls (n = 14). Interestingly, we did not observe an effect following overexpression of FLAG-SZY-20^{dm} (1.2 ± 0.3 fold, n = 12). Thus, the conserved domains that mediate RNA binding in vitro are important for regulating centrosome size.

SZY-20 Limits the Microtubule-Nucleating Capacity of the Centrosome

The microtubule-nucleating capacity of the centrosome positively correlates with the amount of PCM. Since centrosomes in *szy-20(bs52)* embryos contain elevated levels of PCM components, we wondered if such centrosomes nucleate more microtubules. First we analyzed the centrosome level of γ-tubulin,

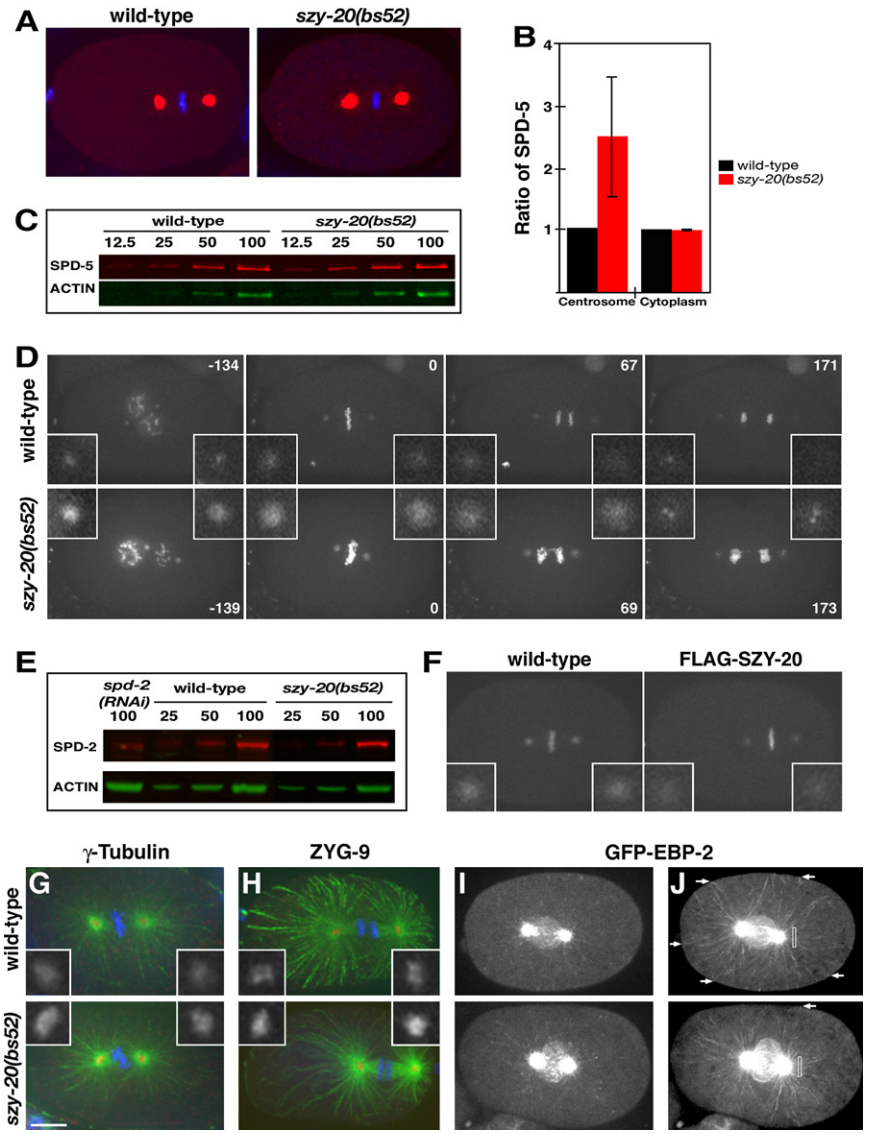

Figure 4. SZY-20 Limits the Size and the Microtubule-Nucleating Capacity of the Centrosome

(A) Embryos at first metaphase stained for SPD-5 (red) and DNA (blue).

(B) Fluorescence intensity measurements of centrosomal and cytoplasmic SPD-5. Vertical bars indicate the standard deviation.

(C) Quantitative immunoblot of SPD-5. Relative loading volumes are indicated above lanes. Actin served as a loading control.

(D) Still images from recordings of embryos expressing GFP-SPD-2 and GFP-histone. Note that in the *szy-20(bs52)* embryo, more chromosomes are present due to polar body extrusion failure and that the metaphase spindle is shorter. Time (in seconds) is relative to metaphase.

(E) Quantitative immunoblot of SPD-2.

(F) Overexpression of wild-type FLAG-SZY-20 reduces GFP-SPD-2 fluorescence at centrosomes.

(G and H) Embryos were stained for microtubules (green), centrosomes (red), and DNA (blue). The levels of (G) γ-tubulin and (H) ZYG-9 are increased at *szy-20(bs52)* centrosomes compared to the wild-type.

(I and J) Time-lapse recordings of embryos expressing GFP-EBP-2. (I) A Z projection of a single time point illustrates the presence of more GFP-EBP-2 at *szy-20(bs52)* centrosomes. (J) Time projections of a 10 s interval show the tracks of growing microtubules. During this period, more microtubules grow to reach the cortex (arrows) in the wild-type than in the mutant. Boxes (6 μm^2) indicate areas used to measure GFP-EBP-2 fluorescence. Each image is a Z projection. Insets are magnified 3-fold. Bar, 10 μm.

a PCM component directly involved in microtubule nucleation (Figure 4G). Similar to other centrosome proteins, γ-tubulin levels at centrosomes are elevated in the mutant (2.5 ± 1.2 fold, n = 14) relative to the wild-type (n = 13).

We next investigated microtubule nucleation using strains expressing GFP-EBP-2, a marker for microtubule plus ends (Srayko et al., 2005). Compared to controls, *szy-20(bs52)* centrosomes exhibit a significant increase in GFP-EBP-2 fluorescence (Figure 4I). We then made time-lapse recordings of embryos expressing GFP-EBP-2. In projected images from these recordings, it was evident that more microtubules grow out from centrosomes in *szy-20(bs52)* than in wild-type embryos (Figure 4J; Figure S6A and Movie S5). As a means of quantifying the difference in the outgrowth of microtubules between the two strains, we measured the intensity of GFP-EBP-2 in an area adjacent to the centrosome. We found that GFP-EBP-2 fluorescence is increased in the mutant (2.0 ± 0.6 fold, n = 8) compared to controls (n = 8), consistent with the presence of more centrosome-associated microtubules in the mutant. Interestingly, microtubule growth appeared stunted in the mutant. In a 10 s interval, many microtubules nucleated by wild-type centrosomes grow out to meet the cortex, while most microtubules nucleated by *szy-20(bs52)* centrosomes grow only a short distance (Figure 4J; Figure S6B and Movie S6). In fact, only about half as many microtubules reach the cortex in *szy-20(bs52)* embryos as in controls. The lack of long microtubules in the mutant is not due to insufficient recruitment of the microtubule-stabilizing protein ZYG-9 (Matthews et al. 1998), as *szy-20(bs52)* centrosomes (n = 16) actually possess more ZYG-9 (1.7 ± 0.7 fold) than controls (n = 24) (Figure 4H). Instead, microtubules grow slower in the mutant (1.1 μm/s) than in the wild-type (1.3 μm/s). Our results are reminiscent of those of Srayko et al. (2005), who found that conditions that favor microtubule polymerization slow the growth rate of individual microtubules, presumably by depleting free tubulin subunits.

SZY-20 Regulates the Level of Centrosome-Associated ZYG-1

Since *szy-20(bs52)* suppresses *zyg-1* mutations, we wondered if the loss of SZY-20 affects the localization of ZYG-1. In immunostained *szy-20(bs52)* embryos, we found that the level of ZYG-1 at the centrosome varies during the cell cycle as it does in the

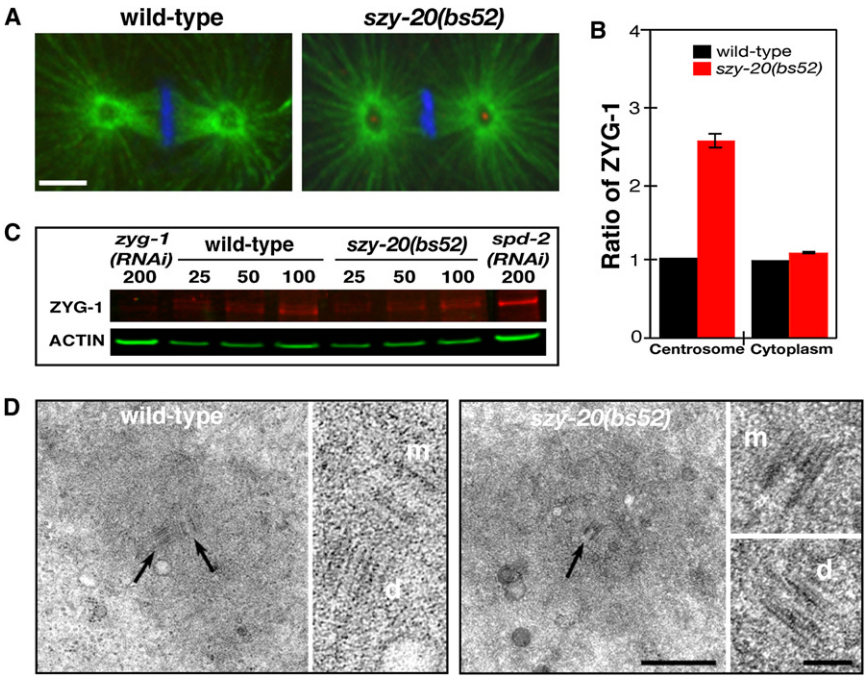

Figure 5. Loss of SZY-20 Activity Enhances ZYG-1 Localization at Centrosomes

(A) Z projections of embryos at first metaphase stained for microtubules (green), ZYG-1 (red), and DNA (blue). ZYG-1 is detectable only at *szy-20(bs52)* centrosomes. Bar, 5 μm.

(B) Fluorescence intensity measurements of centrosomal and cytoplasmic ZYG-1. Vertical bars indicate the standard deviation.

(C) Quantitative immunoblot of ZYG-1. Relative loading volumes are indicated above lanes. Actin served as a loading control.

(D) TEM of centrosomes at anaphase. In the large panels, a wild-type centriole pair (arrows) and the mother centriole (arrow) of a *szy-20(bs52)* centriole pair are shown. In the small panels, all mother (m) and daughter (d) centrioles are shown at higher magnification. Bars, 500 nm for lower and 100 nm for higher magnification images.

wild-type, with the lowest level at metaphase and highest level at anaphase. However, at all cell cycle stages, the level of ZYG-1 is higher at *szy-20(bs52)* centrosomes than at wild-type centrosomes (Figure 5A and Figure S7). This is evident during prometaphase and metaphase, where ZYG-1 was detected in 64% of *szy-20(bs52)* centrosomes (n = 117) but in only 23% of wild-type centrosomes (n = 86). Quantitative fluorescence microscopy at metaphase revealed that *szy-20(bs52)* mutants contain more than twice as much centrosome-associated ZYG-1 as wild-type embryos (Figure 5B). However, we found no difference in the cytoplasmic levels of ZYG-1 between the two strains, suggesting that loss of *szy-20* activity does not simply result in overexpression of ZYG-1. This was confirmed by quantitative immunoblotting (Figure 5C), which found that wild-type and mutant embryos possess equivalent amounts of ZYG-1 (mutant/wt = 1.03 ± 0.12, n = 6). In contrast, we found that depletion of ZYG-1 did not affect SZY-20 localization (data not shown). Thus, SZY-20 regulates ZYG-1 levels at the centrosome but not vice-versa.

As the enlarged centrosomes in *szy-20(bs52)* mutants possess elevated levels of the centriole duplication factor ZYG-1, we wanted to determine if they also possess centrioles of altered structure. Thin section TEM revealed that centrioles are of similar size and structure in wild-type (n = 2) and *szy-20(bs52)* centrosomes (n = 10) (Figure 5D and Figure S8). Thus, the elevated level of PCM observed in *szy-20* mutants appears to occur in the absence of centriole duplication defects.

Centriole Duplication Factors Regulate Centrosome Size

In the course of our analysis, we uncovered an unusual genetic relationship between *zyg-1* and *szy-20*. Not only does *szy-20(bs52)* suppress *zyg-1(it25)*, but the converse is also true (Table 1, top). At 20°C, nearly 100% of the progeny produced by *zyg-1(it25)* hermaphrodites are viable while only 55% of *szy-20(bs52)* embryos are viable. Remarkably, over 90% of the progeny of *zyg-1(it25) szy-20(bs52)* double mutants are viable. This difference between the *szy-20(bs52)* and *zyg-1(it25) szy-20(bs52)* strains is statistically significant ($p < 0.01$); thus, at 20°C loss of *zyg-1* activity restores proper embryonic development to *szy-20(bs52)* mutants.

The mutual suppression exhibited by *zyg-1* and *szy-20* loss-of-function mutations suggests a simple model. A reduction in SZY-20 activity results in increased levels of ZYG-1 at the centrosome, which in turn has deleterious consequences for the embryo. Reducing ZYG-1 activity in the *szy-20(bs52)* mutant could restore an appropriate level of centrosome-associated ZYG-1 and thus normal cellular processes. To analyze the interactions between *zyg-1* and *szy-20* at a cytological level, we performed time-lapse microscopy. At 20°C, *szy-20(bs52)* zygotes exhibit highly penetrant defects in microtubule-dependent processes such as pronuclear rotation (87%, n = 23; Figure 6A) and cytokinesis (63%, n = 19; Movies S3 and S4). In wild-type embryos, the two apposed pronuclei rotate 90° to position the centrosomes and ultimately the spindle on the A-P axis. While this rotation is normally completed by prometaphase in wild-type embryos, it often does not initiate until metaphase in *szy-20(bs52)* embryos. We observed robust rescue of both defects in *szy-20(bs52)* mutants when *zyg-1* activity was reduced. In the *zyg-1(it25) szy-20(bs52)* double mutant, the pronuclear rotation defect is reduced to 12.5% (n = 16) and the cytokinesis defect to 17% (n = 12).

The pronuclear rotation and cytokinesis defects of *szy-20(bs52)* embryos could be a consequence of the enlarged centrosomes. That is, by nucleating more microtubules, the enlarged centrosomes deplete free tubulin and impede the formation of long microtubules that are needed for these processes. If true, suppression of both defects by the *zyg-1(it25)* allele might involve the restoration of centrosome size. To test this, we compared the level of centrosome-associated GFP-SPD-2 in *szy-20(bs52)* and *zyg-1(it25) szy-20(bs52)* zygotes grown at 20°C

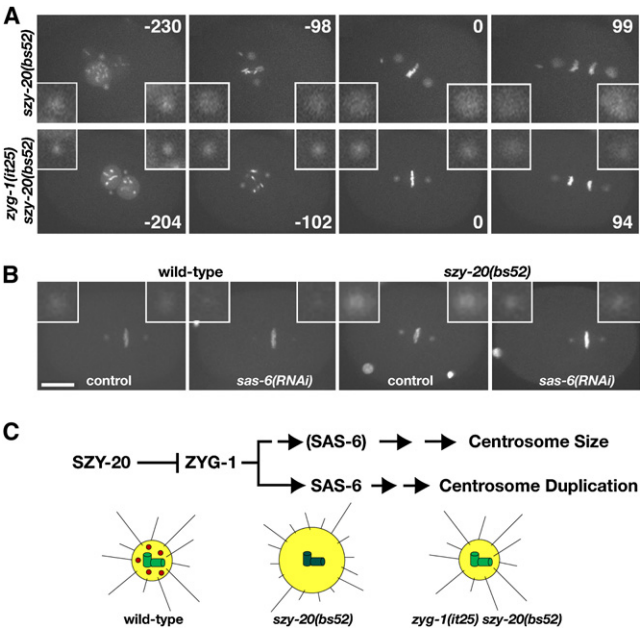

Figure 6. Centriole Duplication Factors Regulate Centrosome Size

(A and B) Images from recordings of embryos expressing GFP-SPD-2 and GFP-histone. (A) Reducing *zyg-1* activity restores normal centrosome size and function to *szy-20(bs52)* mutants. Note that the delay in pronuclear rotation observed in *szy-20(bs52)* is rescued by the *zyg-1(it25)* mutation. Time (seconds) is relative to first metaphase. (B) *sas-6(RNAi)* reduces centrosome size in both wild-type and *szy-20(bs52)* embryos. Shown are Z projections at each time point. Insets are magnified 3-fold. Bar, 10 μm.

(C) A molecular pathway for controlling centrosome size (top). SZY-20 acts upstream and controls the centrosomal level of ZYG-1, which regulates both centrosome duplication and size. The centriole duplication factor SAS-6 also influences centrosome size. It is shown in parentheses in the "Centrosome Size" pathway to indicate that its role here has not yet been firmly established. A depiction of the effects of SZY-20 on the centrosome (bottom). In the wild-type, SZY-20 (red) restricts the amount of ZYG-1 (green) at centrioles, thereby establishing the proper level of PCM (yellow) and microtubules (black lines). In *szy-20* mutants, ZYG-1 levels at centrioles increase, leading to enhanced recruitment of PCM and the nucleation of more microtubules (on average these are shorter than those nucleated by wild-type centrosomes). Reducing ZYG-1 activity in *szy-20* mutants restores normal levels of PCM and microtubule nucleation.

(Figure 6A). Consistent with our prediction, GFP-SPD-2 fluorescence was reduced by nearly half (0.59 ± 0.07) at *zyg-1(it25) szy-20(bs52)* centrosomes (n = 12) compared to *szy-20(bs52)* centrosomes (n = 14). Importantly, these experiments were conducted at 20°C, where centrosome duplication is not blocked by the *zyg-1(it25)* mutation. Thus, the reduction in centrosome size is not a consequence of blocking daughter centriole formation. We further found that in the wild-type, depletion of ZYG-1 by RNAi reduces the level of GFP-SPD-2 at the centrosome by more than half (0.4 ± 0.26 fold, n = 11) relative to controls (n = 10). Therefore, ZYG-1 has two separable functions. It regulates centrosome duplication and controls centrosome size. These results also show that inappropriately high levels of ZYG-1 at the centrosome can perturb centrosome function.

Finally, we investigated whether the ability to regulate centrosome size is shared by other centriole duplication factors. We used RNAi to deplete SAS-6 in both wild-type and *szy-20(bs52)* embryos expressing GFP-SPD-2 (Figure 6B; Figure S9 and Movies S7 and S8). Compared to controls (n = 20), depletion of SAS-6 in *szy-20(bs52)* mutants reduced the amount of GFP-SPD-2 at centrosomes by nearly half (54%, n = 23), an effect similar in magnitude to that produced by depleting ZYG-1 activity. In wild-type embryos, *sas-6(RNAi)* (n = 14) produced an even greater effect, reducing the amount of centrosome-associated GFP-SPD-2 to 40% of controls (n = 11). Interestingly, while *sas-6(RNAi)* invariably blocked centrosome duplication in wild-type embryos, we found it to be much less potent in *szy-20(bs52)* embryos, where centrosomes were often able to duplicate (data not shown). This suggests that the *szy-20(bs52)* mutation can also partially suppress the duplication defect in SAS-6-deficient embryos. Our results thus uncover a second function for ZYG-1, SAS-6, and possibly other centriole assembly factors: to regulate centrosome size.

DISCUSSION

Many factors that participate in assembly of a functional centrosome have been identified. However, the precise roles played by these factors, the order in which they act, and the mechanisms by which the cell determines an appropriate amount of PCM and microtubule-nucleating capacity at each stage of the cell cycle are not completely understood. SZY-20 plays an unusual role in centrosome morphogenesis. Whereas all factors identified to date play a positive role in centrosome assembly, SZY-20 negatively regulates this process.

SZY-20 Links Centrosome Duplication and PCM Recruitment

Our data show that SZY-20 is involved in both centrosome duplication and PCM recruitment. These results confirm and extend previous work on the complex interplay between centrioles and PCM. Disruption of centrioles causes PCM to disperse (Bobinnec et al., 1998), while disruption of PCM hinders centriole duplication (Dammermann et al., 2004). Recently Loncarek et al. (2008) showed that experimentally increasing the size of PCM in vertebrate somatic cells stimulates the overproduction of centrioles. These centrioles arise as singlets within localized densities of PCM, similar to how centrioles arise de novo (Khodjakov et al. 2002). These studies suggest that PCM provides a microenvironment that facilitates centriole assembly, perhaps by concentrating centriole duplication factors around the mother centriole (Dammermann et al., 2004). The centriole, in turn, acts to organize the PCM into a tight focus, thereby restricting the number of daughter centrioles that can form during S phase (Loncarek et al., 2008).

A key finding of our work is that loss of SZY-20 results in both expansion of the PCM and elevated levels of centrosome-associated ZYG-1. This result suggests two possible models for how SZY-20 suppresses centrosome duplication defects. First, suppression may result from concentrating ZYG-1 at centrosomes, thereby facilitating the ability of the mutant protein to execute its function. Since SPD-2 is required to recruit ZYG-1 to the site of centriole assembly (Delattre et al., 2006; Pelletier et al., 2006), the enhanced localization of ZYG-1 may also compensate for a partial loss of SPD-2 activity. Second, suppression could be due to the expansion of PCM, which could enhance the ability

of the centrosome to concentrate the depleted factors around mother centrioles. Although both models are possible, our finding that ZYG-1 is required for the expansion of PCM in *szy-20* mutants argues in favor of the first model. Most likely, loss of SZY-20 results in an elevated level of centrosome-associated ZYG-1, which then enhances recruitment of downstream factors such as SAS-6 and ultimately PCM components. These results highlight the attractive interactions between centrioles and PCM; not only does the PCM attract centriole duplication factors, but as our results show, the reverse is also true.

If centriole amplification can be driven in other systems by the expansion of PCM or Plk4/Sak overexpression (Kleylein-Sohn et al., 2007; Loncarek et al. 2008; Peel et al., 2007; Rodrigues-Martins et al., 2007), why doesn't the *szy-20* mutant overduplicate its centrioles? One obvious answer is that centrosome duplication might be perturbed more easily in some tissues than in others. Consistent with this idea, Peel et al. (2007) found tissue-specific variations in the extent to which centriole amplification could be induced by overexpressing various duplication factors, suggesting that cells differ with respect to how tightly they regulate centriole duplication. It thus seems likely that centrosome duplication in the worm embryo is stringently regulated and that perturbations in ZYG-1 levels and PCM size cannot disrupt the fidelity of this process.

Centriole Duplication Factors Also Function to Determine Centrosome Size

An unexpected outcome of the current study is that control of centrosome size involves the activities of ZYG-1 and SAS-6, two factors whose only known roles are in centriole assembly (Dammermann et al., 2004; Leidel et al., 2005; O'Connell et al., 2001). Partial depletion of either factor reduces the size of centrosomes that form during the first cell cycle of the embryo. This small-centrosome phenotype is distinct from those reported earlier when ZYG-1 and other centriole duplication factors are partially depleted (Delattre et al., 2004; Kirkham et al., 2003; Leidel et al., 2005). In these cases, dramatically undersized centrosomes are observed following a round of defective centrosome duplication in which centrioles of altered structure and reduced size are formed (Kirkham et al., 2003). This particular effect on centrosome size is likely an indirect consequence of structurally defective centrioles.

Our results suggest that components of the centriole duplication pathway have two separable functions: to assemble centrioles and to endow centrioles with the ability to recruit PCM (Figure 6C). This is most evident from the results on partial depletion of ZYG-1 in *szy-20(bs52)* embryos, where we could significantly reduce centrosome size without affecting centrosome duplication (Figure 6A). SAS-6 also appears to be involved in this pathway, as its depletion reduces centrosome size by more than half (Figures 6B and Figure S9). Although some of this reduction might be due to a block in daughter centriole formation, the magnitude of the effect suggests that the ability of the mother centriole to recruit PCM has been impaired. Further, *szy-20(bs52)* embryos contain centrioles of normal structure and size, indicating that the ZYG-1-dependent increase in centrosome size is unlikely due to perturbations in centriole assembly. Finally, ZYG-1 regulates centrosome size through recruitment of SPD-2, a factor that functions both in centrosome duplication and maturation. This is in contrast to recent studies showing that during centriole assembly SPD-2 is required to recruit ZYG-1 but not vice versa (Delattre et al., 2006; Pelletier et al., 2006). This discrepancy likely reflects different pathways under study: the earlier studies dealing with SPD-2 recruitment to the centriole during duplication and our study dealing with recruitment of SPD-2 to the PCM during maturation.

SZY-20 Possibly Functions in RNA Metabolism

Cytological and genetic evidence favor the site of SZY-20 action to be the centrosome itself. Although SZY-20 localizes to a number of structures, its temporal pattern of association with the centrosome is suggestive; at the centrosome, SZY-20 levels peak when ZYG-1 levels are lowest, suggesting that SZY-20 regulates ZYG-1 directly. However, we have not detected a direct physical interaction between ZYG-1 and SZY-20 (unpublished data). While it is not yet known how SZY-20 controls centrosome size and duplication, it seems likely that SZY-20 participates in regulating some aspect of RNA metabolism. SZY-20 contains domains that are found in known RNA-binding proteins. For instance, the *Drosophila* Encore protein, which contains a SUZ domain, associates with other RNA-binding proteins and has been shown to be required for the localization and translation of different maternal mRNAs (Hawkins et al., 1997; Van Buskirk and Schupbach, 2002). In support of a role in RNA metabolism, mutation of the SUZ and SUZ-C domains of SZY-20 disrupts both in vitro RNA-binding activity and centrosome size control.

How would a role in RNA metabolism allow SZY-20 to regulate centrosome size? Recently, a number of RNA and RNA-binding proteins have been shown to be associated with centrosomes and microtubules (Alliegro et al., 2006; Blower et al., 2005, 2007; Groisman et al., 2000; Lambert and Nagy, 2002; Lecuyer et al., 2007). Rae1, an RNA export factor, binds directly to microtubules and plays a role in mitotic spindle assembly (Blower et al., 2005). In *Xenopus*, the protein Maskin, a member of a family of spindle assembly proteins, regulates translation of centrosome-associated cyclin B1 message (Groisman et al., 2000; O'Brien et al., 2005). Also, the transcript of a centrosomal component, D-PLP/CP309 in *Drosophila*, has been reported to localize to centrosomes (Lecuyer et al., 2007). Thus, one intriguing possibility is that SZY-20 might function in the localization, stability, or translation of RNA at the centrosome to locally regulate expression of one or more proteins. Future studies, aimed at identifying interacting molecules, will help elucidate the molecular targets and mechanism of action of SZY-20.

A Balance of SZY-20 and ZYG-1 Activities Regulates the Microtubule-Nucleating Capacity of the Centrosome

szy-20 mutant embryos improperly execute a number of microtubule-dependent processes. As inhibition of *zyg-1* restores both normal centrosome size and microtubule function to *szy-20* mutants, there appears to be a causal relationship between the two. It has been shown that depletion of microtubule-destabilizing factors depresses the rate of microtubule growth in the *C. elegans* embryo (Schlaitz et al., 2007; Srayko et al., 2005). Similarly, when treated with the microtubule-stabilizing agent taxol, *C. elegans* embryos form more but shorter astral microtubules and fail to properly align spindles (Hyman and White, 1987). These defects, which are similar to those observed in

szy-20 mutants, are thought to be due to depletion of free tubulin. This suggests that the cell must carefully balance the levels of free and polymerized tubulin to maintain normal microtubule-dependent processes. SZY-20 appears to regulate this balance at the level of microtubule nucleation and possibly stability, as centrosomes in *szy-20* mutants possess elevated levels of microtubule nucleating (γ-tubulin) and stabilizing (ZYG-9) factors. Our work shows that SZY-20 regulates the level of ZYG-1 at centrosomes and that a delicate balance in the activity of these two factors ensures proper centrosome size and function. When this balance is upset either by inhibiting SZY-20 or ZYG-1 or overexpressing SZY-20, centrosome size is affected in predictable ways.

In summary, our work describes a molecular pathway that is important for regulating centrosome size. This pathway, which depends upon the conserved protein SZY-20, the kinase ZYG-1, and likely other core centriole duplication factors, is functionally distinct from the mechanism of centriole assembly. Our work thus identifies an additional function for centriole duplication factors and provides insight into a molecular mechanism for controlling centrosome size.

EXPERIMENTAL PROCEDURES

Strain Maintenance and Genetics

Worms were cultured on MYOB plates seeded with *E. coli* OP50 (Church et al., 1995). Except for the Hawaiian variant CB4856, all strains were derived from the wild-type Bristol N2 strain. The following mutations were used: LGI: *spd-2(or188ts)*; LGII: *zyg-1(it25ts), zyg-1(or409ts), dpy-10(e128), mnDf68, mnDf104, szy-20(bs52ts), szy-20 (tm1997ts), unc-4(e120)*. The *szy-20(tm1997)* deletion allele was produced by The National BioResource Project, Japan. The following integrated transgenes were used: *bsIs2* [*pCK6.1*: *unc-119(+) pie-1-gfp-spd-2*] (Kemp et al., 2004), *ojIs2* [*pLM6:unc-119(+) pie-1-gfp-tba-1*], and *ruIs32* [*pAZ132: unc-119(+) pie-1-gfp-his-58*] (Praitis et al., 2001). All strains were grown at 16°C or 20°C unless otherwise indicated.

Cloning of *szy-20*

For single-nucleotide polymorphism (SNP) mapping, *dpy-10(e128) szy-20(bs52) unc-4(e120)* hermaphrodites were crossed with CB4856 males. A total of 124 independent Dpy-nonUnc or Unc-nonDpy recombinants were isolated from the F_2 generation. Homozygous recombinant lines were established and scored for the presence of *szy-20(bs52)* by examining embryonic viability at 25°C. SNPs were analyzed by sequencing or by the method of Wicks et al. (2001). Selected ORFs within a region defined by SNP mapping were amplified from *szy-20(bs52)* genomic DNA and sequenced.

Molecular Biology

The EST clones yk658b1, yk1428h04, yk1555h10, and yk1636d07 (gifts from Yuji Kohara) were sequenced to confirm the molecular structure of *szy-20*. The 5′ end of the *szy-20* transcript was amplified from the cDNA library pHS1 (gift of Harold Smith) using primers directed against the *trans*-spliced SL1 leader, 5′-GGTTTAATTACCCAAGTTTGAG-3′, and C18E9.3, 5′-CTCTCC ATAGTGCTCTACCATG-3′.

szy-20(RNAi) was performed by soaking and/or feeding (Wang and Barr, 2005). To produce dsRNA for soaking, we used the primers 5′-ATGAGTAAAG AAAATGTTGTCG-3′ and 5′-CTATTGAGGCCGATTCTGCTGC-3′ to amplify a DNA template from N2 genomic DNA or yk1428h04. Each primer contained the T7 promoter sequence at its 5′ end. Templates were transcribed in vitro using the T7-MEGAscript kit (Ambion). For soaking, L1–L4 larvae were incubated overnight in M9 buffer containing either 0.1–0.4 mg dsRNA/ml or no dsRNA (control). For feeding, larvae were grown on *E. coli* HT115 carrying pMS1.3, an RNAi feeding vector containing the entire *szy-20* genomic sequence. Modifications of the *szy-20* coding region were made using the QuikChange II XL Site-Directed Mutagenesis Kit (Stratagene) according to the manufacturer's instructions. Transgenic lines were produced as described (Praitis et al., 2001).

Protein Sequence and Structure Analysis

Protein complexity analysis was performed with the SEG program (Wootton and Federhen, 1996). The nonredundant (NR) database of protein sequences (National Center for Biotechnology Information, NIH, Bethesda) was searched using the BLASTP program (Altschul et al., 1997). Profile searches were conducted using the PSI-BLAST program with either a single sequence or an alignment used as the query, with a default profile inclusion expectation (E) value threshold of 0.01 (unless specified otherwise), and were iterated until convergence (Altschul et al., 1997). The query sequences were subject to a statistical correction for compositional bias to avoid inflation of significance by low-complexity regions (Schaffer et al., 2001).

Cytology

The following antibodies were used at a 1:500–1:2000 dilution: DM1A (Sigma), α-GFP (Roche), α-SPD-2 (Kemp et al., 2004), α-SPD-5 (Hamill et al., 2002), α-ZYG-1 (O'Connell et al., 2001), α-ZYG-9 (Matthews et al., 1998), and Alexa Fluor 488 and 568 secondary antibodies (Invitrogen). Affinity-purified rabbit polyclonal antibodies were prepared against the following peptides: for SZY-20 (αS20N): Ac-HHKLNQKEKQPAPTYEERQAC-amide; for SAS-4: Ac-MASDENIGADGEQKPSC-amide; for γ-tubulin: Ac-CLSKYDKLRSKRAFIDK-amide.

Indirect immunofluorescence, spinning disk confocal microscopy, and 4D-DIC microscopy were performed as described (Kemp et al., 2007). For confocal microscopy, Openlab software (Improvision, Inc.) was used to acquire images from a Nikon Eclipse E800 microscope equipped with a Plan Apo 100× 1.4 NA lens, a PerkinElmer Ultra*VIEW* spinning disk unit, and a Hamamatsu C9100-12 EM-CCD camera. Image processing was done with Photoshop CS. For 4D-DIC, we used IPLab software to acquire images from a Zeiss Axiovert 200M microscope equipped with a Hamamatsu ORCA-ER camera. Fluorescence intensity measurements were made using ImageJ v1.39e. Electron microscopy was performed as described (Muller-Reichert et al., 2007).

Immunoblotting

Embryos were dissolved in sample buffer, fractionated on a NuPAGE Bis-Tris Gel (Invitrogen), and blotted to nitrocellulose using the iBlot Gel Transfer System (Invitrogen). αS20N, α-SPD-2 (Kemp et al., 2004), α-SPD-5 (Dammermann et al., 2004), α-ZYG-1 (Kemp et al., 2007), DM1A (Sigma), and α-Actin (Novus Biologicals) were used at a 1:500–1:1500 dilution. IRDye secondary antibodies (LI-COR Biosciences) were used at 1:15,000 dilution. Blots were analyzed using the Odyssey Infrared Imaging System (LI-COR Biosciences).

Supplemental Experimental Procedures

Additional experimental details on protein structure analysis, immunostaining, protein expression, and RNA-binding assays can be found in the Supplemental Data.

SUPPLEMENTAL DATA

The Supplemental Data include Supplemental Results, Supplemental Experimental Procedures, nine figures, and eight movies and can be found with this article online at http://www.cell.com/developmentalcell/supplemental/S1534-5807(08)00400-0.

ACKNOWLEDGMENTS

We thank So Jung Kim and O'Connell lab members for their support; David Weisblat, Andy Golden, Bob Goldstein, Nick Miliaras, and Nina Peel for comments on the manuscript; Harold Smith, Martin Srayko, Alexander Dammerman, Anjon Audhya, Karen Oegema, Ken Kemphues, and Yuji Kohara for reagents; and In-Geol Choi and Kevin Eliceiri for technical assistance. Some strains were provided by The *Caenorhabditis* Genetics Center and The National Bioresource Project, Japan. This work was supported by the Intramural Research Program of the National Institutes Health (NIH) and by the National Institute of Diabetes and Digestive and Kidney Diseases.

Received: November 21, 2007
Revised: June 6, 2008
Accepted: September 26, 2008
Published: December 8, 2008

REFERENCES

Alliegro, M.C., Alliegro, M.A., and Palazzo, R.E. (2006). Centrosome-associated RNA in surf clam oocytes. Proc. Natl. Acad. Sci. USA *103*, 9034–9038.

Altschul, S.F., Madden, T.L., Schaffer, A.A., Zhang, J., Zhang, Z., Miller, W., and Lipman, D.J. (1997). Gapped BLAST and PSI-BLAST: a new generation of protein database search programs. Nucleic Acids Res. *25*, 3389–3402.

Azimzadeh, J., and Bornens, M. (2007). Structure and duplication of the centrosome. J. Cell Sci. *120*, 2139–2142.

Bettencourt-Dias, M., Rodrigues-Martins, A., Carpenter, L., Riparbelli, M., Lehmann, L., Gatt, M.K., Carmo, N., Balloux, F., Callaini, G., and Glover, D.M. (2005). SAK/PLK4 is required for centriole duplication and flagella development. Curr. Biol. *15*, 2199–2207.

Blower, M.D., Nachury, M., Heald, R., and Weis, K. (2005). A Rae1-containing ribonucleoprotein complex is required for mitotic spindle assembly. Cell *121*, 223–234.

Blower, M.D., Feric, E., Weis, K., and Heald, R. (2007). Genome-wide analysis demonstrates conserved localization of messenger RNAs to mitotic microtubules. J. Cell Biol. *179*, 1365–1373.

Bobinnec, Y., Khodjakov, A., Mir, L.M., Rieder, C.L., Edde, B., and Bornens, M. (1998). Centriole disassembly in vivo and its effect on centrosome structure and function in vertebrate cells. J. Cell Biol. *143*, 1575–1589.

Church, D.L., Guan, K.L., and Lambie, E.J. (1995). Three genes of the MAP kinase cascade, mek-2, mpk-1/sur-1 and let-60 ras, are required for meiotic cell cycle progression in *Caenorhabditis elegans*. Development *121*, 2525–2535.

Dammermann, A., Muller-Reichert, T., Pelletier, L., Habermann, B., Desai, A., and Oegema, K. (2004). Centriole assembly requires both centriolar and pericentriolar material proteins. Dev. Cell *7*, 815–829.

Delattre, M., Leidel, S., Wani, K., Baumer, K., Bamat, J., Schnabel, H., Feichtinger, R., Schnabel, R., and Gonczy, P. (2004). Centriolar SAS-5 is required for centrosome duplication in *C. elegans*. Nat. Cell Biol. *6*, 656–664.

Delattre, M., Canard, C., and Gonczy, P. (2006). Sequential protein recruitment in *C. elegans* centriole formation. Curr. Biol. *16*, 1844–1849.

Dix, C.I., and Raff, J.W. (2007). *Drosophila* Spd-2 recruits PCM to the sperm centriole, but is dispensable for centriole duplication. Curr. Biol. *17*, 1759–1764.

Giansanti, M.G., Bucciarelli, E., Bonaccorsi, S., and Gatti, M. (2008). Drosophila SPD-2 is an essential centriole component required for PCM recruitment and astral-microtubule nucleation. Curr. Biol. *18*, 303–309.

Gomez-Ferreria, M.A., Rath, U., Buster, D.W., Chanda, S.K., Caldwell, J.S., Rines, D.R., and Sharp, D.J. (2007). Human Cep192 is required for mitotic centrosome and spindle assembly. Curr. Biol. *17*, 1960–1966.

Groisman, I., Huang, Y.S., Mendez, R., Cao, Q., Theurkauf, W., and Richter, J.D. (2000). CPEB, maskin, and cyclin B1 mRNA at the mitotic apparatus: implications for local translational control of cell division. Cell *103*, 435–447.

Habedanck, R., Stierhof, Y.D., Wilkinson, C.J., and Nigg, E.A. (2005). The Polo kinase Plk4 functions in centriole duplication. Nat. Cell Biol. *7*, 1140–1146.

Hamill, D.R., Severson, A.F., Carter, J.C., and Bowerman, B. (2002). Centrosome maturation and mitotic spindle assembly in *C. elegans* require SPD-5, a protein with multiple coiled-coil domains. Dev. Cell *3*, 673–684.

Hawkins, N.C., Van Buskirk, C., Grossniklaus, U., and Schupbach, T. (1997). Post-transcriptional regulation of gurken by encore is required for axis determination in *Drosophila*. Development *124*, 4801–4810.

Hyman, A.A., and White, J.G. (1987). Determination of cell division axes in the early embryogenesis of Caenorhabditis elegans. J. Cell Biol. *105*, 2123–2135.

Kemp, C.A., Kopish, K.R., Zipperlen, P., Ahringer, J., and O'Connell, K.F. (2004). Centrosome maturation and duplication in *C. elegans* require the coiled-coil protein SPD-2. Dev. Cell *6*, 511–523.

Kemp, C.A., Song, M.H., Addepalli, M.K., Hunter, G., and O'Connell, K. (2007). Suppressors of zyg-1 define regulators of centrosome duplication and nuclear association in *Caenorhabditis elegans*. Genetics *176*, 95–113.

Khodjakov, A., Rieder, C.L., Sluder, G., Cassels, G., Sibon, O., and Wang, C.L. (2002). De novo formation of centrosomes in vertebrate cells arrested during S phase. J. Cell Biol. *158*, 1171–1181.

Kirkham, M., Muller-Reichert, T., Oegema, K., Grill, S., and Hyman, A.A. (2003). SAS-4 is a *C. elegans* centriolar protein that controls centrosome size. Cell *112*, 575–587.

Kleylein-Sohn, J., Westendorf, J., Le Clech, M., Habedanck, R., Stierhof, Y.D., and Nigg, E.A. (2007). Plk4-induced centriole biogenesis in human cells. Dev. Cell *13*, 190–202.

Lambert, J.D., and Nagy, L.M. (2002). Asymmetric inheritance of centrosomally localized mRNAs during embryonic cleavages. Nature *420*, 682–686.

Lecuyer, E., Yoshida, H., Parthasarathy, N., Alm, C., Babak, T., Cerovina, T., Hughes, T.R., Tomancak, P., and Krause, H.M. (2007). Global analysis of mRNA localization reveals a prominent role in organizing cellular architecture and function. Cell *131*, 174–187.

Leidel, S., and Gonczy, P. (2003). SAS-4 is essential for centrosome duplication in *C. elegans* and is recruited to daughter centrioles once per cell cycle. Dev. Cell *4*, 431–439.

Leidel, S., Delattre, M., Cerutti, L., Baumer, K., and Gonczy, P. (2005). SAS-6 defines a protein family required for centrosome duplication in *C. elegans* and in human cells. Nat. Cell Biol. *7*, 115–125.

Loncarek, J., Hergert, P., Magidson, V., and Khodjakov, A. (2008). Control of daughter centriole formation by the pericentriolar material. Nat. Cell Biol. *10*, 322–328.

Luders, J., and Stearns, T. (2007). Microtubule-organizing centres: a re-evaluation. Nat. Rev. Mol. Cell Biol. *8*, 161–167.

Matthews, L.R., Carter, P., Thierry-Mieg, D., and Kemphues, K. (1998). ZYG-9, a *Caenorhabditis elegans* protein required for microtubule organization and function, is a component of meiotic and mitotic spindle poles. J. Cell Biol. *141*, 1159–1168.

Muller-Reichert, T., Srayko, M., Hyman, A., O'Toole, E.T., and McDonald, K. (2007). Correlative light and electron microscopy of early *Caenorhabditis elegans* embryos in mitosis. Methods Cell Biol. *79*, 101–119.

O'Brien, L.L., Albee, A.J., Liu, L., Tao, W., Dobrzyn, P., Lizarraga, S.B., and Wiese, C. (2005). The Xenopus TACC homologue, maskin, functions in mitotic spindle assembly. Mol. Biol. Cell *16*, 2836–2847.

O'Connell, K.F., Caron, C., Kopish, K.R., Hurd, D.D., Kemphues, K.J., Li, Y., and White, J.G. (2001). The *C. elegans* zyg-1 gene encodes a regulator of centrosome duplication with distinct maternal and paternal roles in the embryo. Cell *105*, 547–558.

Peel, N., Stevens, N.R., Basto, R., and Raff, J.W. (2007). Overexpressing centriole-replication proteins in vivo induces centriole overduplication and de novo formation. Curr. Biol. *17*, 834–843.

Pelletier, L., Ozlu, N., Hannak, E., Cowan, C., Habermann, B., Ruer, M., Muller-Reichert, T., and Hyman, A.A. (2004). The *Caenorhabditis elegans* centrosomal protein SPD-2 is required for both pericentriolar material recruitment and centriole duplication. Curr. Biol. *14*, 863–873.

Pelletier, L., O'Toole, E., Schwager, A., Hyman, A.A., and Muller-Reichert, T. (2006). Centriole assembly in *Caenorhabditis elegans*. Nature *444*, 619–623.

Praitis, V., Casey, E., Collar, D., and Austin, J. (2001). Creation of low-copy integrated transgenic lines in *Caenorhabditis elegans*. Genetics *157*, 1217–1226.

Rodrigues-Martins, A., Riparbelli, M., Callaini, G., Glover, D.M., and Bettencourt-Dias, M. (2007). Revisiting the role of the mother centriole in centriole biogenesis. Science *316*, 1046–1050.

Schaffer, A.A., Aravind, L., Madden, T.L., Shavirin, S., Spouge, J.L., Wolf, Y.I., Koonin, E.V., and Altschul, S.F. (2001). Improving the accuracy of PSI-BLAST protein database searches with composition-based statistics and other refinements. Nucleic Acids Res. *29*, 2994–3005.

Schlaitz, A.L., Srayko, M., Dammermann, A., Quintin, S., Wielsch, N., MacLeod, I., de Robillard, Q., Zinke, A., Yates, J.R., 3rd, Muller-Reichert, T.,

et al. (2007). The *C. elegans* RSA complex localizes protein phosphatase 2A to centrosomes and regulates mitotic spindle assembly. Cell *128*, 115–127.

Srayko, M., Kaya, A., Stamford, J., and Hyman, A.A. (2005). Identification and characterization of factors required for microtubule growth and nucleation in the early *C. elegans* embryo. Dev. Cell *9*, 223–236.

Stein, K.K., Davis, E.S., Hays, T., and Golden, A. (2007). Components of the spindle assembly checkpoint regulate the anaphase-promoting complex during meiosis in *Caenorhabditis elegans*. Genetics *175*, 107–123.

Van Buskirk, C., and Schupbach, T. (2002). Half pint regulates alternative splice site selection in *Drosophila*. Dev. Cell *2*, 343–353.

Wang, J., and Barr, M.M. (2005). RNA interference in *Caenorhabditis elegans*. Methods Enzymol. *392*, 36–55.

Wicks, S.R., Yeh, R.T., Gish, W.R., Waterston, R.H., and Plasterk, R.H. (2001). Rapid gene mapping in *Caenorhabditis elegans* using a high density polymorphism map. Nat. Genet. *28*, 160–164.

Wootton, J.C., and Federhen, S. (1996). Analysis of compositionally biased regions in sequence databases. Methods Enzymol. *266*, 554–571.

Zhu, F., Lawo, S., Bird, A., Pinchev, D., Ralph, A., Richter, C., Muller-Reichert, T., Kittler, R., Hyman, A.A., and Pelletier, L. (2008). The mammalian SPD-2 ortholog Cep192 regulates centrosome biogenesis. Curr. Biol. *18*, 136–141.